# Tunneling conductance of a magnetized zigzag graphene nanoribbon/superconductor junction

J. Wang, L. Zhang, and K. S. Chan

*Department of Physics, Southeast University, Nanjing 210096, China, People's Republic of China and Department of Physics and Materials Science, City University of Hong Kong, Tat Chee Avenue, Kowloon, Hong Kong, People's Republic of China*

(Received 17 October 2010; revised manuscript received 20 December 2010; published 28 March 2011)

The zigzag graphene nanoribbon (ZGNR) has very peculiar electronic structure and transport properties such as the edge state, spontaneous magnetization, and the even-odd effect. In this work, we report a theoretical study on the interplay between the magnetization and pseudoparity of the particle, and their combined effect on the tunneling conductance spectra of the ZGNR/superconductor junction. It is shown that the magnetization in ZGNR can significantly modify the original even-odd effect in nonmagnetic ZGNR due to the definite pseudoparity of the particles. For the ferromagnetic ZGNR that can be obtained by an external magnetic field or the proximity effect through a ferromagnet on ZGNR, the Andreev reflection (AR), which is entirely prohibited in the nonmagnetic ZGNR with an even zigzag chain number, is now allowed only for one kind of spin; thus the system resembles a spin-diode device in which only one spin species AR can occur under positive bias while the other spin species AR occurs under negative bias. For the antiferromagnetic ZGNR with weak magnetization, the conductance gap appears at Fermi energy due to the insulating property of ZGNR; in addition, AR is also possible for the even ZGNR, and two conductance peaks appear in the superconductor energy gap, which is attributed to the pseudoparity of the edge state destroyed by the antiferromagnetic ordering in ZGNR. For the odd ZGNR, either ferromagnetic or antiferromagnetic magnetization has no qualitative influence on the conductance spectra of the junction. Our findings may shed light on devising spin devices based on magnetized graphene nanoribbons.

DOI: 10.1103/PhysRevB.83.125425 PACS number(s): 72.10.−d, 74.45.+c, 73.23.−b

## I. INTRODUCTION

Recent progress in experimental fabrication of a single layer of graphite, graphene, has led to extensive exploration of electronic properties and novel transport phenomena in this material.[1–21] Graphene is a one-atom-thick layer of carbon atoms tightly packed into a honeycomb crystal lattice whose symmetries lead to a linear energy-momentum relation for the low-energy quasiparticles, which can be described by the massless relativistic Dirac equation. Owing to the unique band structure, graphene has many peculiar properties, such as the specular Andreev reflection in a normal/superconductor (SC) junction,[5] Klein tunneling[6] related to the chiral nature of the quasiparticle, the unconventional half-integer quantum Hall effect,[7,8] and the realization of superlenses by focusing of electron beams[9]. Due to the weak spin-orbit coupling[10] and low hyperfine interaction,[11] its spin relaxation length can reach the order of micrometers at room temperature. In addition, graphene has also extremely high mobility and very long mean free path[1,12] at room temperature, so that it could be an excellent candidate for microelectronic applications as well as for spintronic applications.

The graphene nanoribbon (GNR), a strip of graphene with its width in nanometers, has also been extensively studied by researchers since it may be the building block of future graphene-based electronic devices. Two basic nanoribbons are mostly studied, the edge of GNR pointing along the C-C bond is referred to as the armchair GNR, while the edge perpendicular to the C-C bond is the zigzag GNR. The zigzag graphene nanoribbon (ZGNR) has very peculiar electronic and transport properties due to the zero-energy edge state localized at two edges of the ribbon.[13] Within the wave vector $2\pi/3 < ka < 4\pi/3$, the edge states are highly degenerate and thus unstable, and the spontaneous magnetization, lattice distortion, or charge polarization may occur at the edges of ZGNR to stabilize the system.[14] Both the *ab initio*[14–18] and tight-binding model calculations[13,19–21] have shown that the ground state of ZGNR is an antiferromagnetic (AFM) band insulator, i.e., the magnetization at two edges are antiparallel to each other while it keeps ferromagnetic ordering along in each edge, so that there is no net magnetization in the system. With the help of a transverse electric field, the ground state of ZGNR could even be a half-metal[15] in which one spin channel is conductive whereas the other keeps insulating.

Besides the AFM structure, the ferromagnetic (FM) magnetic ordering has often been studied in ZGNR, and it is a metallic state. The first-principle calculations[14,17] have demonstrated that the energy of FM-ZGNR is slightly higher than that of AFM-ZGNR,[14] e.g., as $N = 8$, their energy difference is estimated $\Delta E \sim 25$ meV, and exhibits a power-law decay with the width of ribbon $1/N^{1.8}$, where $N$ is the number of zigzag chains in the ZGNR. Therefore, the FM structure would be easily stabilized by applying an experimentally accessible magnetic field or through the proximity effect from an FM metal on ZGNR.[22] Since the AMF-ZGNR is an insulator whereas the FM-ZGNR is metallic, such properties of ZGNR were studied by many authors[23–26] to develop the efficient magnetoresistance (MR) device; e.g., Rojas *et al.*[23] suggested that the application of an external magnetic field on ZGNR should transform the AFM ground state into the FM metallic state, and the system's resistance would drastically change, thus a very high MR could be realized.

Another remarkable property of ZGNR, the current-blocking effect or valley-valve effect,[27–30] has also been investigated by many authors; the wave function of a particle at the $K$ valley or $K'$ valley can exhibit the same or different pseudoparity that depends on whether $N$ is even or odd. In the ZGNR p-n junction with even $N$, the particle transmission could be entirely prohibited because the injected and transmitted

 

particle within the single energy-mode has a different pseudoparity. This valley-valve effect was also proposed to realize high-performance MR[31–33] or a spin filter device;[32] e.g., Kim *et al.*[31] found that two parallel or antiparallel FM metal electrodes deposited on ZGNR can induce the FM ordering in the ribbon so that the spin-dependent current blocking effect can result in 100% MR at low bias. Zhang *et al.*[32] found the FM-ZGNR with even $N$ could be a perfect spin-filter device if only a single mode is involved in transport, that is, only one spin channel is open and the other spin channel is closed. Certainly, such a spin-filter effect is just a spin-polarized version of the current-blocking effect and is feasible in the FM p-n junction.

So far, the interplay between the magnetization and pseudoparity of the particle in ZGNR as well as their combined effect on the transport property lacks enough attention, thus in this work, we study the tunneling conductance spectra of the magnetized ZGNR/SC junction (SC, $s$-wave superconductor) by considering both the edge magnetization and even-odd parity effect. Rainis *et al.*[34] have investigated the same junction without consideration of any magnetization, and they found that in the even ZGNR, the Andreev reflection (AR) is totally prohibited, while it is allowed in the odd ZGNR, which is a typical even-odd effect due to the pseudoparity of the particle. When the magnetization of ZGNR is turned on, the case would be very different and the pseudoparity of the particle could also be altered, which in turn results in remarkable influence on the electron transport properties.

In a tight-binding model, we calculate the magnetization of ZGNR self-consistently within the mean-field approximation as well as the spin-dependent conductance of the ZGNR/SC junction with the help of the Keldysh Green's function. It is found that for the even FM-ZGNR, the junction behaves like a spin-diode device where only one spin species AR can occur for positive bias while the opposite spin species AR is allowed for negative bias. For the AFM-ZGNR, the conductance gap appears at Fermi energy due to its insulating energy gap, while at very weak AFM magnetization, AR is also possible for even ZGNR and two conductance peaks appear in the SC energy gap because the pseudoparity of the edge states are destroyed by the AFM magnetic ordering.

This paper is organized in the following way. In the second section, we introduce first the lattice Hubbard model describing ZGNR with on-site Coulomb interaction, and then reduce it by the Hartree-Fock approximation. The Keldysh Green's function is used to derive the tunneling conductance of the junction. In the third section, the self-consistent calculation of the magnetization distribution on lattice sites is presented, and the spin-resolved conductance for both FM-ZGNR/SC and AFM-ZGNR/SC junctions are calculated. In the last section, some discussions on the obtained results are given and a brief conclusion is drawn.

## II. MODEL AND FORMULA

The two-dimension ZGNR/SC junction is schematically shown in Fig. 1, it consists of the left ZGNR lead, the right SC lead, and the middle transitional ZGNR region in the box, where the damping magnetization from the left ZGNR lead is considered. $N$ is the number of zigzag chains, $N_x$ is the number of unit cells in the middle ZGNR region, and $a = \sqrt{3}a_0$ ($a_0 = 1.42$Å) is the lattice constant of graphene. The following model Hamiltonian is employed here to describe the junction:

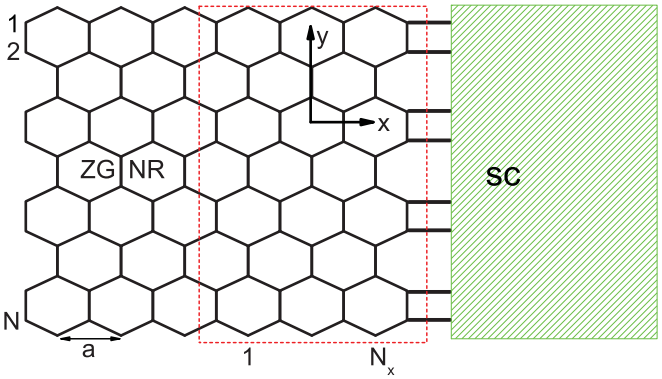


FIG. 1. (Color online) Planar hybrid junction consisting of the left ZGNR and right SC lead in the $xy$ plane. $N$ is the number of zigzag chains in the ZGNR, $N_x$ is the number of unit cells in the ZGNR within the red-dashed-line box connecting with the SC lead.

$$H = H_L + H_R + H_{LR}, \tag{1}$$

where $H_L$ and $H_R$ describe the graphene ribbon region and the SC lead, respectively; $H_{LR}$ is the coupling between the ZGNR and SC lead. In the tight-binding representation,[19] $H_L$ is given by

$$H_L = \sum_{i\sigma} \varepsilon_i C^\dagger_{i\sigma} C_{i\sigma} - t \sum_{\langle ij\sigma\rangle} (C^\dagger_{i\sigma} C_{j\sigma} + \text{c.c.}) + U \sum_{i\sigma} (n^\dagger_{i\sigma} n_{i\bar{\sigma}}), \tag{2}$$

where $C^\dagger_{i\sigma}$ ($C_{i\sigma}$) is the creation (annihilation) operator at the site $i$ with spin $\sigma$ ($\sigma = \pm = \uparrow\downarrow$), $\bar{\sigma} = -\sigma$, $\langle ij\rangle$ denotes the summation over the nearest neighbor sites, $t$ is the hopping integral, and $\varepsilon_i$ is the on-site energy and equals zero for the undoped graphene, which can simulate potentials from static defects or impurities; the last term is the on-site Hubbard term with $U$ being the Coulomb interaction constant, and $n_{i\sigma}$ is the $\sigma$-spin electron operator on site $i$. $H_L$ describes also the middle ZGNR region that may have different site potentials $\varepsilon_i$ and site electron $\langle n_{i\sigma}\rangle$ from the left lead.

The right lead can be either a metal SC electrode or a graphene SC in which the SC pair potential in the ribbon comes from the SC proximity effect. Here the metal SC lead is employed, and it does not have the honeycomb lattice structure of graphene. In a continuum model, the $s$-wave SC is given by

$$H_R = \sum_{k\sigma} (\varepsilon_k - \mu) b^\dagger_{k\sigma} b_{k\sigma} + \sum_k (\Delta b^\dagger_{k\uparrow} b^\dagger_{-k\downarrow} + \Delta b_{-k\downarrow} b_{k\uparrow}), \tag{3}$$

where $b^\dagger_{k\sigma}$ ($b_{k\sigma}$) is the creation (annihilation) operator in the superconductor lead with the momentum $\mathbf{k} = (k_x, k_y)$, $\Delta$ is the real pair potential constant and the macroscopic SC phase is neglected here, and $\mu$ is the chemical potential. The Hamiltonian $H_{LR}$ is the coupling term connecting ZGNR and the SC lead

$$H_{LR} = \sum_{i\sigma} t' C^\dagger_{i\sigma} b_{i\sigma} + \text{H.c.} \tag{4}$$

Here $b_{i\sigma}$ is the lattice version of the operator $b_{k\sigma}$ in the SC lead, $t'$ is the coupling strength and the spin is conserved when quasiparticles tunnel between ZGNR and SC. It is noted that the site index $i$ denotes only the surface site connecting SC and ZGNR.

To deal with the Coulomb interaction in $H_L$, the unrestricted Hartree-Fock approximation (HFA) method is employed here so that it can be transformed into a single-electron Hamiltonian as

$$H_L = \sum_{i\sigma}(\varepsilon_i + U\langle n_{i\bar{\sigma}}\rangle)\, C^{\dagger}_{i\sigma}C_{i\sigma} - t\sum_{\langle ij\sigma\rangle}(C^{\dagger}_{i\sigma}C_{j\sigma} + \text{c.c.}) + U\sum_{i\sigma}\langle n_{i\bar{\sigma}}\rangle\langle n_{i\bar{\sigma}}\rangle, \tag{5}$$

where $\langle n_{i\sigma}\rangle$ is the statistical average electron occupation on site $i$ with spin $\sigma$, and needs to be computed self-consistently,

$$\langle n_{i\sigma}\rangle = \int \rho_{i\sigma}(E) f(E)\, dE, \tag{6}$$

where $\rho_{i\sigma}(E)$ is the density of states (DOS) of the $\sigma$-spin electron on site $i$ and $f(E)$ is the Fermi distribution function. In the equation above, it can be seen that the electron-electron interaction in HFA induces an additional effective exchange potential $U\langle n_{i\sigma} - n_{i\bar{\sigma}}\rangle$. The density of states can be worked out with the energy dispersion determined by the single-electron Hamiltonian Eq. (5).

The spin-dependent current flowing through the ZGNR/SC junction can be worked out by the evolution of the total number of electrons operator $N_\sigma$ at the surface sites of ZGNR, $I_\sigma = e\partial N_\sigma/\partial t = \frac{e}{i\hbar}[N_\sigma, H]$, it is then given by

$$I_\sigma = \frac{e}{\hbar}\int \frac{dE}{2\pi}\text{Tr}\big[G^r_\sigma(E)\Sigma^<_{L\sigma} + G^<_\sigma(E)\Sigma^a_{L\sigma} + \text{H.c.}\big]_{11}, \tag{7}$$

where the trace is over the transverse lattice site $i$ at the interface between the left ZGNR lead and the middle ZGNR region, the subscript 11 denotes the electron component of the Numbu space, $G^<_\sigma(E)$ is the matrix Green's function in the Nambu space and it is the Fourier transformation of $G^<_\sigma(t,t')$:

$$G^<_{ij,\sigma}(t,t') = i\begin{pmatrix}\langle C^+_{j\sigma}(t')C_{i\sigma}(t)\rangle & \langle C_{j\bar{\sigma}}(t')C_{i\sigma}(t)\rangle \\ \langle C^+_{j\sigma}(t')C^+_{i\bar{\sigma}}(t)\rangle & \langle C_{j\bar{\sigma}}(t')C^+_{i\bar{\sigma}}(t)\rangle\end{pmatrix}, \tag{8}$$

with $C_{i\sigma}$ ($C_{j\sigma}$) being the electron operator in the ZGNR, the dimension of $G^<$ is $4NN_x \times 4NN_x$ with $2N$ the site number of a unit cell of ZGNR, $\bar{\sigma}$ denotes the hole component of the Nambu space, while the $\sigma$ spin denotes the electron component. Since there is no nonlinear spin-related interaction and the spin-up and spin-down space is independent, we can work out the spin-up and spin-down quantities separately. $\Sigma^{r(<)}_{L\sigma}$ is the retarded (lesser) self-energy of the left lead, and they are given by

$$\Sigma^r_{L\sigma}(E) = \begin{pmatrix}\tilde{t}_{ij}g_{11\sigma}\tilde{t}^{\dagger}_{ij} & 0 \\ 0 & \tilde{t}^*_{ij}g_{22\bar{\sigma}}(\tilde{t}^*_{ij})^{\dagger}\end{pmatrix}, \tag{9}$$

and

$$\Sigma^<_\sigma(E) = \begin{pmatrix}if^+(E)\Gamma_{L\sigma}(E) & 0 \\ 0 & if^-(E)\Gamma_{L\bar{\sigma}}(E)\end{pmatrix}, \tag{10}$$

where $f^{\pm}(E) = f(E \mp eV)$ with $V$ being the applied voltage, $g_{11(22)}$ is the electron (hole) component of the surface Green's function of the left ZGNR lead, which can be obtained by a simple iteration method, $\tilde{t}_{ij}$ is the coupling term between the two neighboring unit cells of ZGNR, and $i\Gamma_{L\sigma} = \Sigma^a_{L\sigma} - \Sigma^r_{L\sigma}$. By using the Keldysh equation $G^< = G^r\Sigma^<G^a$, $G^r - G^a = iG^r\Gamma G^a$, the spin-dependent current in Eq. (7) is reduced to

$$I_\sigma = \frac{e}{\hbar}\int\frac{dE}{2\pi}\text{Tr}\{\Gamma_{L\sigma}[G^r\Gamma_R G^a]_{11}\}(f^+ - f) + \text{Tr}\{\Gamma_{L\sigma}G^r_{12\sigma}\Gamma_{L\bar{\sigma}}G^a_{21,\sigma}\}(f^+ - f^-), \tag{11}$$

where the $G^{r(a)}$ is the retarded (advanced) Green's function, which can be obtained by the direct matrix inversion

$$G^r = [EI - H_m - \Sigma^r]^{-1} \tag{12}$$

and $G^a = [G^r]^{\dagger}$, where $H_m$ is the Hamiltonian of the center region in the Nambu space, $I$ is the unit matrix, and $\Sigma^{ra<} = \Sigma^{ra<}_L + \Sigma^{ra<}_R$. $\Sigma^r_R$ is the self-energy of the right SC lead[35] that reads

$$\Sigma^r_R = -i\Gamma_0 J_0\big(k_F(y_i - y_j)\big)\beta(E)\begin{pmatrix}1 & \Delta/E \\ \Delta/E & 1\end{pmatrix}, \tag{13}$$

where $\beta(E) = |E|/\sqrt{E^2 - \Delta^2}$ with $|E| > \Delta$ and $\beta(E) = E/i\sqrt{\Delta^2 - E^2}$ with $|E| > \Delta$, and $J_0$ is the first-kind Bessel function. In the derivation of Eq. (11), the formula $\Sigma^<_R = (\Sigma^a_R - \Sigma^r_R)f(E)$ is also used. In the linear transport regime, $eV \sim \Delta \ll E_F$, the spin-resolved conductance is given by

$$G_\sigma = \frac{2e^2}{h}\text{Tr}[\Gamma_{L\sigma}[G^r\Gamma_R G^a]_{11}] + \frac{e^2}{h}\text{Tr}\big[\Gamma_{L\sigma}G^r_{12\sigma}\Gamma_{L\bar{\sigma}}G^a_{21,\sigma}\big], \tag{14}$$

where the first term is the AR coefficient and the second term is the quasiparticle's tunneling coefficient; the former dominates in the energy gap $|eV| < \Delta$ while the latter contributes to the current when $|eV| > \Delta$.

Before we calculate the conductance $G_\sigma$ of the junction, we turn to present the definition of the pseudoparity of the particle in Ref. 29, which is very useful in the following analysis of the conductance spectra. For a uniform ZGNR, The eigenvector of a unit cell is the linear superposition of the atom-orbital Bloch wave function, and they are given by

$$\Psi(\mathbf{k},\mathbf{r}) = \sum_{i=1}^{2N}\alpha_i\Phi_i(\mathbf{k},\mathbf{r}), \tag{15}$$

and

$$\Phi_i(\mathbf{k},\mathbf{r}) = \frac{1}{\sqrt{M}}\sum_{\mathbf{R}_m} e^{i\mathbf{k}\cdot(\mathbf{R}_m + \mathbf{d}_i)}\phi_z(\mathbf{r} - \mathbf{R}_m - \mathbf{d}_i), \tag{16}$$

where $\mathbf{R}_m$ is lattice vector of the $m$th cell in ZGNR, $\mathbf{d}_i$ is the position of the $i$th ($1 \leqslant i \leqslant 2N$) carbon atom in a unit cell of ZGNR, $\phi_z$ is the local atom-orbital wave function of the $\pi$-electron, and $\alpha_i$ is the superposition coefficient and can be worked out by simply directly solving the eigenvectors of the single-electron $H_L$. Owing to the lattice structure symmetry of ZGNR, the coefficient $\alpha_i$ fulfills the following relation as

$$\alpha^n_i(\mathbf{k}) = (-1)^p\alpha^n_{2N+1-i}(\mathbf{k}), \tag{17}$$

where $p$ is referred to as the pseudoparity and can be even or odd depending on the energy level $n$ as well as the wave vector $\mathbf{k}$.

## III. RESULTS

### A. Magnetization in ZGNR

We first study the magnetic structure of a uniform ZGNR based on Eq. (5), the hopping energy is taken as $t = 2.8$ eV, the Coulomb constant is set $U = 1t$ from the *ab initio* calculation,[14] the temperature is $T = 0$ K, and the Fermi wave vector[35] for the SC lead is set $k_F = 1\text{Å}^{-1}$. The pair potential is set as $\Delta = 1$ meV and the line width $\Gamma_0 = 0.1$ eV. For the self-consistent calculation within HFA, the initial guess of the electron occupation on each site with certain magnetic ordering is needed, and then the energy dispersion is then obtained as well as a new electron occupation from Eq. (6), which is input again into Eq. (5) for calculating density of state. Such iteration procedure will not end until the final results are convergent within endurable accuracy. Both the AFM and FM ordering state in ZGNR could be obtained with the initial assumption of the corresponding magnetic structure. Note that the undoped ZGNR is considered here with the site energy $\varepsilon_i = 0$, so each site has only one $\pi$ electron on average.

In Fig. 2, the local magnetization distribution denoted by $\langle n_{i\uparrow} - n_{i\downarrow}\rangle$ at each site of a unit cell is presented, where the magnetic moment $\mu_B$ is taken as unity. The AFM structure is shown in Fig. 2(a) and the magnetization mainly localizes in two edge atoms and rapidly damps into the inside of ZGNR, which indicates that the magnetization should stem from the edge states. The magnetization directions at the two edges are antiparallel to each other with same magnitude, that is, the AFM ordering forms in the unit cell but the FM ordering exists along two edges, and there is no net magnetization in the

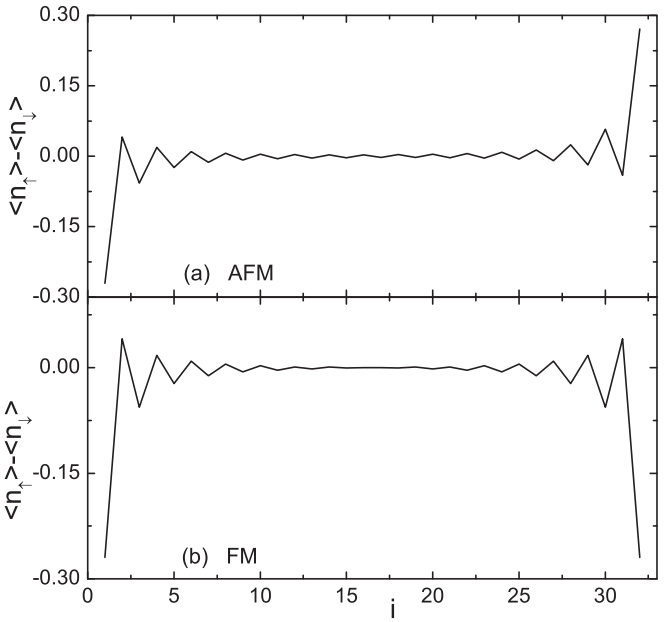


FIG. 2. Magnetization ($\langle n_\uparrow\rangle - \langle n_\downarrow\rangle$) at each transverse site $i$ of both (a) AFM-ZGNR and (b) FM-ZGNR. The Coulomb constant $U = 1t$ and $N = 16$; other parameters are described in text.

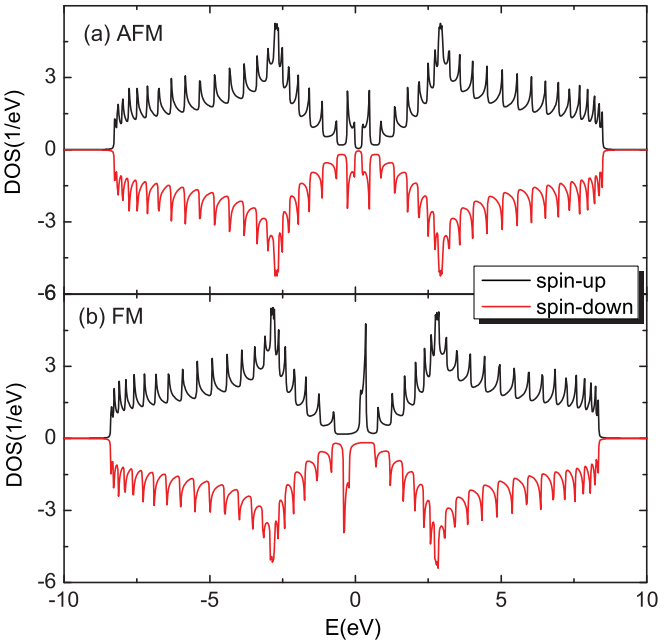


FIG. 3. (Color online) Spin-resolved density of states for (a) AFM-ZGNR and (b) FM-ZGNR. The Coulomb constant $U = 1t$ and $N = 16$; the negative density of states is meaningless and denotes the opposite spin-species DOS to that of the positive DOS.

system. The spin-resolved density of states of the AFM-ZGNR are plotted in Fig. 3(a), where each peak corresponds to the subband energy level of ZGNR and an energy gap appears at the Fermi level ($E_F = 0$); the edge states around $E_F$ are spin-split due to the AFM exchange coupling. Therefore, the AFM-ZGNR is a band insulator, and the magnitude of the energy gap depends on the ratio of $U/t$ and the ribbon width $N$. Generally, the larger Coulomb interaction $U$ and narrower $N$ ZGNR favor a larger energy gap as well as the larger magnetization. The first-principle calculation[16,17] proved the energy band gap $\delta$ is inversely proportional to the width $N$, $\delta \sim 9.33eV/(w_z + 15)$ with $w_z$ the ribbon width in angstroms.

For the self-consistent iteration, the FM structure in ZGNR could also be worked out by assuming an initial FM electron distribution in the ZGNR lattice, and similarly, this FM magnetic ordering is readily convergent. In Fig. 2(b), the local magnetization distribution on the transverse sites is presented, and at two edges the magnetizations stay parallel to each other with equal values. Same as the AFM magnetization, the magnetic moment in Fig. 2(b) attenuates rapidly from two edges into the inner; certainly, the FM-ZGNR has a net magnetic moment in the system. The magnitude of the edge magnetization in FM (0.27) is a little smaller than that of AFM (0.28), whereas its total energy per unit cell ($E_{\text{tot}} = -56.78$ eV) is a little larger than that of AFM ($E_{\text{tot}} = -56.89$ eV). In Fig. 3(b), the spin-resolved DOSs are also plotted, and the finite DOSs appear at $E_F$, i.e., the FM-ZGNR is metallic; the edge states are spin-split and one spin is shifted above $E_F$ and the other below $E_F$, thus the spin-resolved edge states may lead to very different transport properties due to the different pseudoparity of the particle, as discussed below.

Both FM and AFM magnetic structures are possible solutions of the Hubbard model and they are more stable

than the nonmagnetic solution,[14] while the AFM structure is energetically more favorable than the FM structure. However, the energy difference is very small and decreases with the width of ZGNR $N$, which were verified by the *ab initio* numerical calculations.[14,17] Therefore, the FM structure could be stabilized readily by small magnetic field or depositing an FM metal on the ribbon. In the following calculation of the tunneling conductance, both the FM and AFM magnetic ordering in ZGNR are considered. Given the strong magnetization in a narrower ZGNR that can strongly suppress AR coefficient and lead to the larger energy gap in the AFM-ZGNR, the very weak magnetization in the same magnitude of order as the SC energy gap $\Delta$ is considered to simulate the much wider ZGNR. This is done by using small Coulomb constant $U$ in the self-consistent iteration, since the wider ZGNR has a much weaker magnetization as well as smaller AFM band gap. It is estimated that the width of ZGNR is on the order of 100 nm so that the spin exchange energy is on the order of SC energy gap meV. We wish to point out that the smaller $U$ used here to simulate the wider ZGNR will not change the pseudoparity of the particle and the properties of the edge state of ZGNR.

### B. FM-ZGNR/SC junction

In last section, we recovered two magnetic structures in ZGNR in the tight-binding model, the obtained electron distribution is input in Eq. (5) as a starting point to calculate the tunneling conductance. For comparison, we first present the conductance of the nonmagnetic ZGNR/SC junction, which was studied in Ref. 34.

In Fig. 4, where the conductance $G$ is plotted, the AR dominates in the SC energy gap $|eV| < \Delta$ while the quasiparticle tunneling contributes to the current at $|eV| > \Delta$. As is shown, for the odd ZGNR, the conductance $G$ at both $|eV| > \Delta$ and

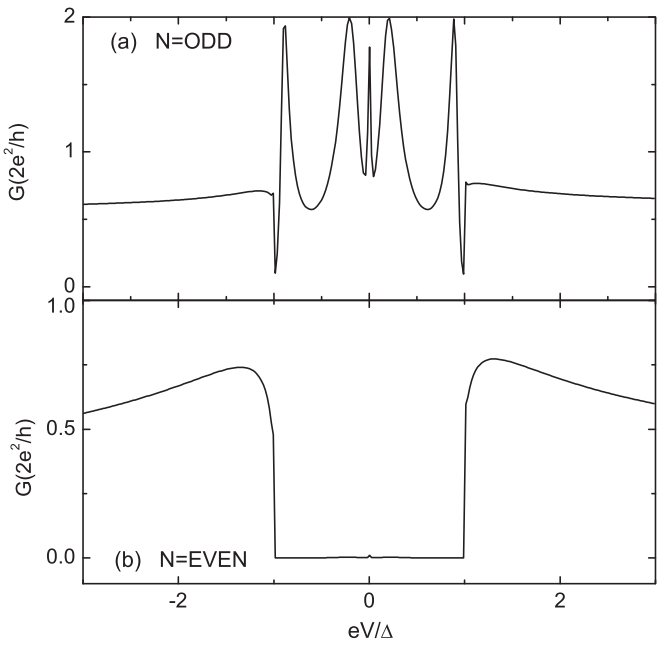


FIG. 4. Spin-degenerate conductance of the nonmagnetic ZGNR/SC junction for (a) the odd case $N = 15$, and (b) the even case $N = 16$; $N_x = 5$.

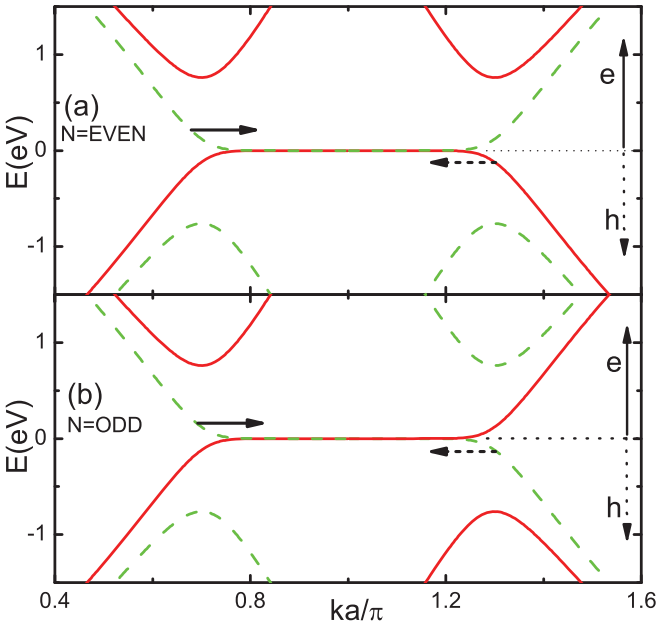


FIG. 5. (Color online) Two energy levels of the nonmagnetic ZGNR near Fermi energy as a function of the longitudinal wave vector $ka/\pi$. The electron band is plotted for $E > 0$ and the hole band is at $E < 0$, the green dash line denotes the even parity of the particle, while the red line stands for the odd parity. The right solid arrow stands for the injected electron-like quasiparticle; the left dotted arrow is for the reflected hole-like quasiparticle. (a) $N = 16$ for the even ZGNR and (b) $N = 15$ for odd ZGNR.

$|eV| < \Delta$ regime is nonzero, the AR coefficient equals unity only at the resonant points. While for the even ZNGR, the AR is entirely suppressed and the nonzero conductance comes from the quasiparticle tunneling with $eV > \Delta$. Such conductance spectra have been interpreted according to the pseudoparity of the quasiparticle in Ref. 34. In Fig. 5, the energy dispersion of the quasiparticle in ZGNR with corresponding pseudoparity is shown for the levels around $E_F$. For the even ZGNR in Fig. 5(a), the injected electron-like quasiparticle has different pseudoparity from that of the reflected hole-like quasiparticle, so that this AR is prohibited; i.e., the two electron with different parity cannot compose a Cooper pair entering the SC lead. In Fig. 5(b), the odd ZGNR is plotted, the injected electron-like quasiparticle and reflected hole-like particle has same pseudoparity, so that the AR is allowed.

It is noted that the results shown in Fig. 4 are valid only in single energy mode transport, and the AR is also allowed for the even ZGNR when more subbands of ZGNR are involved in transport. However, for the mesoscopic ZGNR/SC junction, the subband energy gap is much larger than the SC energy gap $\Delta$, so that only the zero-energy edge state contributing to the current is reasonable for small bias. For instance, the SC $\Delta$ is in magnitude of $10k_BT \sim 1$ meV, while the energy gap between the first subband and zeroth band in ZGNR is estimated[36] to be 8 meV for the width of ZGNR $w \sim 120$ nm by using the formula $\Delta E \sim t\pi/(N + 1/2)$.

We now proceed to study the FM magnetic ordering effect on the tunneling conductance of the ZGNR/SC junction. To avoid suppressing the conductance due to the strong spin exchange splitting, the weak magnetization is adopted

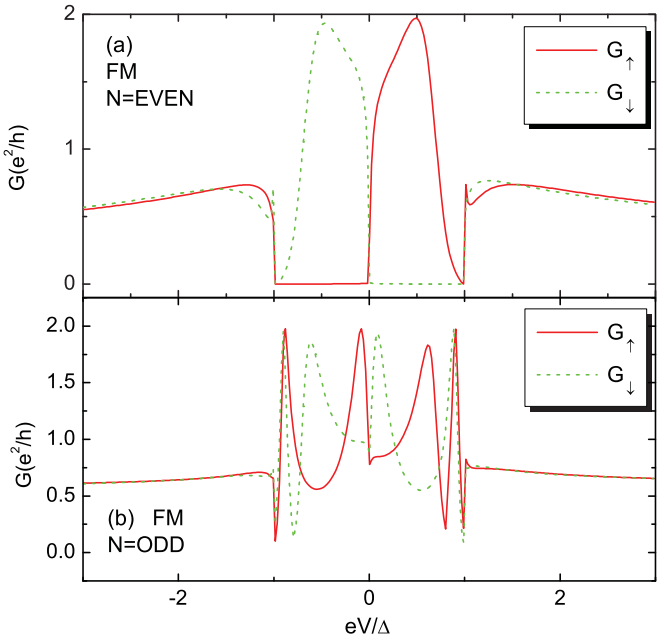


FIG. 6. (Color online) Spin-resolved conductances of the FM-ZGNR/SC junction for both even and odd cases, (a) $N = 16$ and (b) $N = 15$. The Coulomb constant is set at $U = 0.1t$ and the magnetization at edge atom is obtained as $(\langle n_\uparrow\rangle - \langle n_\downarrow\rangle) = 0.00452$ with $N = 16$, and $(\langle n_\uparrow\rangle - \langle n_\downarrow\rangle) = 0.00458$ with $N = 15$.

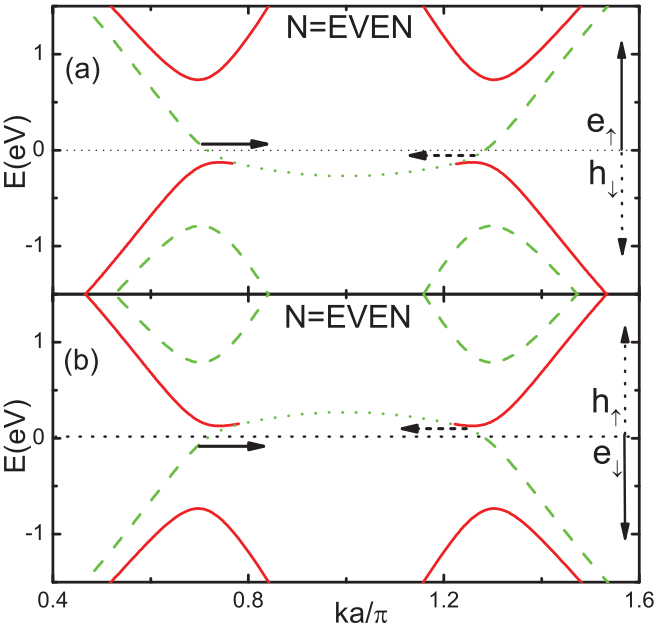


FIG. 7. (Color online) Two energy levels of the FM-ZGNR near the Fermi energy as a function of the longitudinal wave vector $ka/\pi$ with even number of zigzag chain $N = 16$. (a) The spin-up electron band, which is across $E_F$ due to the FM spin splitting, is plotted for $E > 0$ and the spin-down hole band ($E < 0$) overlaps to the spin-up electron band, and they have the same pseudoparities, the dotted green line denotes the energy dispersion of the spin-down hole quasiparticle, which has the same pseudoparity of the green dash line at $E > 0$, and the Andreev reflection is possible between them as indicated by the solid and dotted arrows. (b) The spin-down electron band overlaps with spin-up hole band (dotted line) with the same pseudoparity, and they are across $E_F$ due to the FM spin splitting, the Andreev reflection is possible between them as indicated by solid and dotted arrow.

here as stated earlier. The uniform magnetization in the left semi-infinite ZGNR lead is considered, the linear decrease of the magnetization is assumed in the middle region and vanishes at the right interface between the ribbon and the SC. It is expected that the magnetization at the boundary near the SC should become vanishing since the Cooper pair leaking from the SC lead is antagonistic to the magnetism. In Fig. 6, the spin-dependent conductances $G_{\uparrow(\downarrow)}$ are plotted, and the AR is not suppressed for the even-ZGNR case in comparison with Fig. 4(b), while $G_{\uparrow(\downarrow)}$ for the odd-ZGNR case has no much difference from that of the nonmagnetic junction in Fig. 4(a), the AR is allowed in the energy gap. As stated above, the different pseudoparity of the injected electron-like quasiparticle and reflected hole-like quasiparticle prohibits the AR process for the even ZGNR. However, it is not the case when the FM magnetization in ZGNR is considered. It is shown in Fig. 6(a) that one spin species (say, spin-up) AR is allowed, whereas the other spin species (spin-down) AR is suppressed with $eV > 0$; while for negative bias $eV < 0$, the opposite spin species AR is allowed or suppressed. It is a spin-diode effect that only one spin channel is active and the other spin channel is closed at positive bias, and the opposite case occurs for negative bias.

To interpret this phenomena, the energy dispersion of the particle is also plotted in Fig. 7 for the even ZGNR. It is noted that both the electron and hole band intersect the Fermi energy due to spin splitting, this could be seen in Fig. 3(b). The hole band is obtained by operating the mirror inversion[37] of the electron band over $E_F$ since there is no SC energy gap in ZGNR. For example, the spin-down hole band in Fig. 7(a) at $E < 0$ is acquired from the spin-down electron band at $E > 0$ (not shown). Note the curves with $E > 0$ in Fig. 7(a) comes from the spin-up electron band. Because of the special structure of graphene, the spin-down hole band is exactly overlapped with the spin-up electron band, therefore, the dotted line at $E < 0$ in Fig. 7(a) is used to denote the hole band curve.

Dueto the FM spin splitting, spin-up and spin-down electron bands are split, and both spin bands are across the Fermi level ($E_F = 0$). In Fig. 7(a), the spin-up electron band at $E > 0$ and the spin-down hole band at $E < 0$ are presented, the latter comes from the mirror inversion of the spin-down electron band. Now the AR is possible only between the injected electron-like quasiparticle and the reflected hole-like quasiparticle indicated by solid and dotted arrows in Fig. 7(a), since they have the same pseudoparities. The spin-down electron-like quasiparticle in the left ZGNR lead with $E > 0$ cannot contribute to the current because its pseudoparity is different from that in the transition ZGNR region where the magnetization decreases to zero gradually. Therefore, only the spin-up AR is now allowed at $eV > 0$ for the even ZGNR. The same analysis is also applicable to the spin-down electron-like quasiparticle injection at $eV < 0$; it is specially noted that the spin-down electron band [Fig. 7(b)] across $E_F$ comes from the original $E < 0$ energy level branch at zero magnetization. In the same sense, the AR is allowed because the spin-down electron band overlaps with the spin-up hole band and they possess the same pseudoparity, as shown in Fig. 7(b).

In all, for the even ZGNR, the FM spin splitting is the reason that only one spin species AR is possible for positive or negative bias, in other words, only the energy level across the $E_F$ contributes to the AR process whereas the level deviating from $E_F$ does not. Moreover, the energy band of the injected electron-like quasiparticle and reflected hole-like particle are exactly overlapped to each other, and importantly, they have the same pseudoparity.

### C. AFM-ZGNR/SC junction

In this section, we proceed to check the AFM magnetization effect on the tunneling conductance of the ZGNR/SC junction. As stated early, the AFM magnetic ordering is the ground state of ZGNR and is energetically favorable over the FM state; however, it is a band insulator so the conductance would be zero if the band gap is comparatively large. Therefore, a very weak magnetization resulting in a small band gap is considered in calculations. Similarly, the weak Coulomb constant is employed in the numerical calculations as above.

The spin-resolved conductances $G_{\uparrow(\downarrow)}$ are shown in Fig. 8 for both the even and odd ZGNR. As expected, $G_{\uparrow(\downarrow)}$ exhibits a conductance gap at $E_F$ for both cases due to the insulating band gap. It is seen that two conductance peaks appear in the SC energy gap for the even ZGNR, that is, the AR is not fully suppressed and allowed only for a small energy interval; for the odd ZGNR, in comparison with the nonmagnetic ZGNR, there is no much difference except for the conductance gap.

To explain the conductance spectra of the AFM-ZGNR/SC junction, both the electron and hole band of ZGNR are plotted in Fig. 9. The clear characteristic is the band gap at $E_F$. By

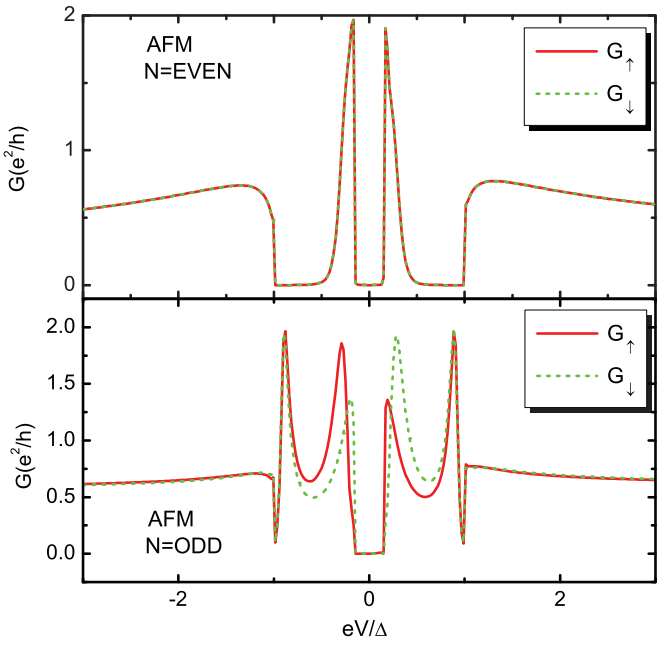


FIG. 8. (Color online) Spin-resolved conductances of the AFM-ZGNR/SC junction for both the even $N = 16$ and odd $N = 15$ cases. The Coulomb constant $U = 0.1t$ and the magnetization at edge atom is obtained as $(\langle n_\uparrow\rangle - \langle n_\downarrow\rangle) = 0.00523$ with $N = 16$, and $(\langle n_\uparrow\rangle - \langle n_\downarrow\rangle) = 0.00492$ with $N = 15$.

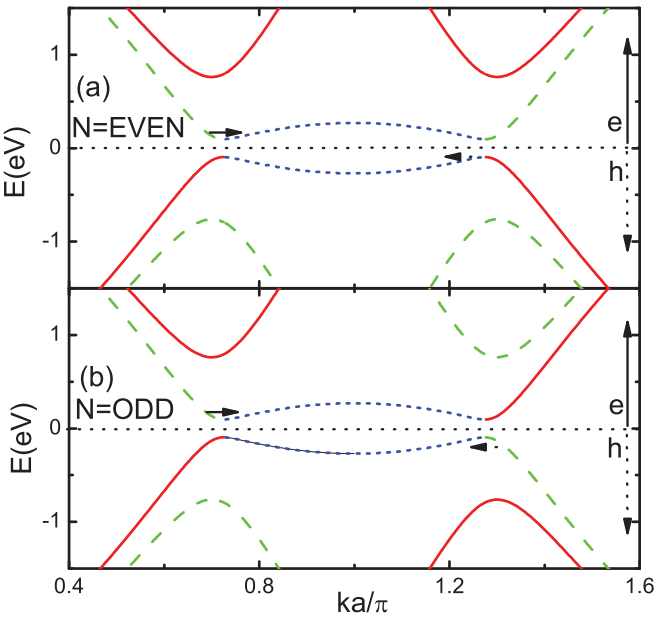


FIG. 9. (Color online) Two energy levels of the AFM-ZGNR near the Fermi energy as a function of the longitudinal wave vector $ka/\pi$; (a) the even ZGNR with $N = 16$, the blue dotted line denotes the nonparity of the edge state, so that the AR is possible only for the energy region of the edge state; (b) the odd-ZGNR case with $N = 15$.

calculating the eigenvectors of a uniform AFM-ZGNR, we found that unlike the nonmagnetic or FM ZGNR, Eq. (17) is no longer valid for the AFM-ZGNR and thus there is no definite so-called pseudoparity. However, for the very weak AFM magnetization, Eq. (17) is nearly valid as $-2\pi/3 < ka < 2\pi/3$, whereas it is nearly invalid as $2\pi/3 < ka < 4\pi/3$ where the edge states exist. In other words, the definite pseudoparity of the edge state is severely destroyed with wave vectors fulfilling $2\pi/3 < ka < 4\pi/3$, while for $-2\pi/3 < ka < 2\pi/3$, the particle has the approximate pseudoparity same as the FM or nonmagnetic ZGNR. The nonparity or parity mixing for the edge state is indicated by the blue dash line in Fig. 9.

For the nonmagnetic even ZGNR, the AR is suppressed because the injected electron-like and reflected hole-like quasiparticles have different pseudoparities as shown in Figs. 4 and 5. When the AFM is turned on in the even ZGNR, there is no definite pseudoparity at $2\pi/3 < ka < 4\pi/3$, the AR is thus possible only for the energy at the wave-vector regime $2\pi/3 < ka < 4\pi/3$, subsequently, the conductance peaks appear at the SC energy gap as shown in Fig. 8(a). As is known, the edge state exists at $2\pi/3 < ka < 4\pi/3$ and it is very flat, so that the allowed energy interval for AR is much narrower. For the odd-ZGNR case in Fig. 9(b), AR is allowed except for the band gap of AFM-ZGNR, the two middle conductance peaks are not spin degenerate, and it is also attributed to the nonparity of the split edge states for $2\pi/3 < ka < 4\pi/3$.

The pseudoparity of the particle in ZGNR is defined according to Eq. (17) and originates from the spatial structure symmetry of ZGNR. In fact, the even and odd ZGNR have very different spatial symmetry, e.g., the odd-ZGNR structure

possesses $C_2$ symmetry, while the even ZGNR has $C_{2h}$ symmetry with an extra reflection symmetry over the rotating axis ($x$ axis). This structure difference leads to the different pseudoparity of the particle even with the same energy, the edge state is an example. When the magnetization is taken into account in ZGNR, the situation may change. For the FM-ZGNR, the structure symmetry plus the spin configuration keep the pseudoparity unchanged; whereas for AFM-ZGNR, the two-fold rotation symmetry is destroyed, therefore, the particle has no longer the definite parity according to Eq. (17). In Fig. 9, we show the nonparity region mainly exists at wave-vector region $2\pi/3 < ka < 4\pi/3$, while the particle with wave vector $-2\pi/3 < ka < 2\pi/3$ has the approximate pseudoparity, the reason is that only the edge states are involved in the transport, and only in this regime $2\pi/3 < ka < 4\pi/3$ does the significant AFM magnetization localize at two edges, which in turn destroys the original structure symmetry of AFM-ZGNR and the pseudoparity. For the $-2\pi/3 < ka < 2\pi/3$ region, the AFM magnetization is so infinitesimal that the pseudoparity of the particle cannot be destroyed severely.

## IV. DISCUSSION AND CONCLUSION

In this work, the magnetization and pseudoparity of a quasiparticle in a ZGNR have been discussed within the tight-binding model and mean-field method, and the interplay between them on the tunneling conductance of the ZGNR/SC junction was investigated in detail by the Keldysh Green's function, with both the FM and AFM magnetic ordering in ZGNR taken into account.

The lattice structure of ZGNR results in formation of the peculiar edge state that localizes mainly at two edges of the ribbon with the wave vector $2\pi/3 < ka < 4\pi/3$, while the energy band for the edge state is nondispersive and highly degenerate, so that the spontaneous magnetization can appear to stabilize the system. In the tight-binding model and HFA, we have investigated both the AFM and FM magnetic ordering in ZGNR; the AFM structure is energetically more favorable than the FM structure, especially for a very narrower ribbon. Since their energy difference per unit cell decreases in power with the width of ribbon $N$, the FM structure in a wider ZGNR is readily stabilized by an external magnetic field or the FM proximity effect, and the FM metal can be either deposited on the ribbon[31] or attached at the edges of the ribbon.[32]

Another peculiar property of ZGNR is that the wave function of the particle has the definite pseudoparity, and moreover, the particle in the even or odd ZGNR with the same energy may possess different pseudoparity, which originates essentially from the lattice structure symmetry. As was analyzed in last section, the even ZGNR has $C_{2h}$ symmetry while the odd ZGNR lacks the reflection symmetry over $x$ axis. The pseudoparity is the origin of the current blocking effect in the even ZGNR[28,29] and the suppression of the AR in the even-ZGNR/SC junction.[34] When the AFM magnetic ordering is considered, the wave function of the particle has no the definite pseudoparity since the magnetizations at two edges are opposite and the $C_2$ symmetry is destroyed, which can thus make a difference on the transport property of ZGNR. More importantly, the magnetization mainly localizes at the edge atoms of ZGNR within $2\pi/3 < ka < 4\pi/3$, so that the so-called pseudoparity of the edge state is severely invalid.

For both the AFM and FM structures, a weak magnetization is assumed in our calculation; for one thing, a strong magnetization would suppress strongly the conductance since the $s$-wave SC is considered and the magnetism is unfavorable for AR as well as quasiparticle tunneling; for another thing, the narrower ZGNR is difficult to fabricate in experiment and the wider ZGNR will significantly reduce the magnetization; moreover, the unavoidable edge defects in ZGNR can also weaken the magnetization. In our calculations, the weak magnetization is realized by assuming a small Coulomb constant, because the self-consistent calculation of the magnetization distribution in a much wider ZGNR, say $w_z = 100$ nm, is too formidable and time consuming. We have also checked the results with the magnetization added in lattice by hand, one assumption is from Ref. 38 that only the edge atoms are magnetized while other inner atoms of ZGNR are spin degenerate, the second assumption is that the magnetization decreases linearly from the edge atom to the middle atom as done in Ref. 32. With these assumed magnetization distributions, the conductance spectra of the ZGNR/SC junction remain essentially unchanged, same as those shown in Figs. 7 and 9. Besides, we have also checked the right SC with the same honeycomb structure as ZNGR, i.e., the superconductivity in the right graphene ribbon lead comes from the proximity effect, and we found the qualitative results presented in this work are also valid.

In summary, we have investigated the magnetization effect on the tunneling conductance of the ZGNR/SC junction by using the Keldysh Green's function method. It was found that for the FM-ZGNR with an even number of zigzag chains in the ribbon, the magnetization can release the suppressed AR and the junction resembles a spin-diode device; only one spin species AR can occur for positive bias while the other spin species AR occurs for the negative bias. For the odd ZGNR, the FM magnetic structure does not change conductance qualitatively. When the AFM magnetic ordering is taken into account in ZGNR, the conductance gap appears at $E_F$ since the AFM-ZGNR is a band insulator, moreover, AR is also possible and two conductance peaks appear in the SC energy gap for even ZGNR, because the pseudoparity of the edge state is severely destroyed, so that the suppression of AR from the pseudoparity for even ZGNR is removed. Our findings may shed light on the interplay between the magnetization and pseudoparity of a particle in the ZGNR and are helpful for devising spin devices based on magnetized graphene nanoribbon.

## ACKNOWLEDGMENTS

This work is supported by City University of Hong Kong Strategic Grant (project no. 7008108). Wang acknowledges support from the NSFC 110704032, 110704033, NSFC of JiangSu Province (BK2010416), and the National Basic Research Project of China (2009CB945504).

[1]K. S. Novoselov, A. K. Geim, S. V. Morozov, D. Jiang, Y. Zhang, S. V. Dubonos, I. V. Grigorieva, and A. A. Firsov, Science **306**, 666 (2004).
[2]Y. Zhang, Y. W. Tan, H. L. Stormer, and P. Kim, Nature (London) **438**, 201 (2005).
[3]K. S. Novoselov, A. K. Geim, S. V. Morozov, D. Jiang, M. I. Katsnelson, I. V. Grigorieva, S. V. Dubonos, and A. A. Firsov, Nature (London) **438**, 197 (2005).
[4]J. R. Williams, L. Dicarlo, and C. M. Marcus, Science **317**, 638 (2007).
[5]C. W. J. Beenakker, Phys. Rev. Lett. **97**, 067007 (2006); Rev. Mod. Phys. **80**, 1337 (2008).
[6]M. I. Katsnelson, K. S. Novoselov, and A. K. Geim, Nat. Phys. **2**, 620 (2006).
[7]K. Yang, Solid State Commun. **143**, 27 (2007).
[8]D. A. Abanin, P. A. Lee, and L. S. Levitov, Phys. Rev. Lett. **96**, 176803 (2006).
[9]J. B. Pendry, Science **315**, 1226 (2007).
[10]C. L. Kane and E. J. Mele, Phys. Rev. Lett. **95**, 226801 (2005).
[11]O. V. Yazyev, Nano Lett. **8**, 1011 (2008).
[12]K. I. Bolotin, K. J. Sikes, Z. Jiang, G. Fudenberg, J. Hone, P. Kim, and H. L. Stormer, Solid State Commun. **146**, 351 (2008).
[13]M. Fujita, K. Wakabayashi, K. Nakada, and K. Kusakabe, J. Phys. Soc. Jpn. **65**, 1920 (1996).
[14]L. Pisani, J. A. Chan, B. Montanari, and N. M. Harrison, Phys. Rev. B **75**, 064418 (2007).
[15]Y.-W. Son, M. L. Cohen, and S. G. Louie, Nature (London) **444**, 347 (2006).
[16]Y.-W. Son, M. L. Cohen, and S. G. Louie, Phys. Rev. Lett. **97**, 216803 (2006).
[17]H. Lee, Y.-W. Son, N. Park, S. Han, and J. Yu, Phys. Rev. B **72**, 174431 (2005).
[18]S. Okada and A. Oshiyama, Phys. Rev. Lett. **87**, 146803 (2001).
[19]Q. Liang, Y. Yu, Q. H. Wang, and J. Dong, Phys. Rev. Lett. **101**, 187002 (2008).
[20]J. Fernandez-Rossier, Phys. Rev. B **77**, 075430 (2008).
[21]M. Wimmer, I. Adagideli, S. Berber, D. Tomanek, and K. Richter, Phys. Rev. Lett. **100**, 177207 (2008).
[22]H. Haugen, D. Huertas-Hernando, and A. Brataas, Phys. Rev. B **77**, 115406 (2008).
[23]F. Munoz-Rojas, J. Fernandez-Rossier, and J. J. Palacios, Phys. Rev. Lett. **102**, 136810 (2009).
[24]R. Qin, J. Lu, L. Lai, J. Zhou, H. Li, Q. Liu, G. Luo, L. Zhao, Z. Gao, W. N. Mei, and G. Li, Phys. Rev. B **81**, 233403 (2010).
[25]S. Honda, A. Yamamura, T. Hiraiwa, R. Sato, J. Inoue, and H. Itoh, Phys. Rev. B **82**, 033402 (2010).
[26]J. C. Chen, S. G. Cheng, S. Q. Shen, and Q. F. Sun, J. Phys. Condens. Matter **22**, 035301 (2010).
[27]A. Rycerz, J. Tworzydlo, and C. W. J. Beenakker, Nat. Phys. **3**, 172 (2007).
[28]A. R. Akhmerov, J. H. Bardarson, A. Rycerz, and C. W. J. Beenakker, Phys. Rev. B **77**, 205416 (2008).
[29]A. Cresti, G. Grosso, and G. P. Parravicini, Phys. Rev. B **77**, 233402 (2008).
[30]K. Wakabayashi and T. Aoki, Int. J. Mod. Phys. B **16**, 4897 (2002).
[31]W. Y. Kim and K. S. Kim, Nat. Nanotechnol. **3**, 408 (2008).
[32]Y. T. Zhang, H. Jiang, Q. F. Sun, and X. C. Xie, Phys. Rev. B **81**, 165404 (2010).
[33]Z. P. Niu and D. Y. Xing, Eur. Phys. J. B **73**, 139 (2010).
[34]D. Rainis, F. Taddei, F. Dolcini, M. Polini, and R. Fazio, Phys. Rev. B **79**, 115131 (2009).
[35]Q. F. Sun and X. C. Xie, J. Phys. Condens. Matter **21**, 344204 (2009).
[36]A. Cresti, G. Grosso, and G. P. Parravicini, Phys. Rev. B **77**, 115408 (2008).
[37]S. Kawabata, Y. Asano, Y. Tanaka, A. A. Golubov, and S. Kashiwaya, Phys. Rev. Lett. **104**, 117002 (2010).
[38]G. Usaj, Phys. Rev. B **80**, 081414(R) (2009).